arXiv:1202.4852v1 [hep-ph] 22 Feb 2012

Rapidity and Transverse Mass Spectra of Hadrons in a New Excluded-Volume Model II

S. K. Tiwari*, P. K. Srivastava, and C. P. Singh

Department of Physics, Banaras Hindu University, Varanasi 221005, INDIA

Abstract

Remarkable success gained by various thermal and statistical approaches in describing the particle multiplicities and their ratios has emphasized the formation of a fireball consisting of chemically equilibrated hot and dense hadron gas (HG) produced in the ultrarelativistic heavy-ion collisions. In an earlier paper referred as I, we proposed a thermodynamically consistent excluded-volume model for the HG fireball and we noticed that the model gives a suitable description for various properties of multiparticle production and their ratios in the entire range of temperatures and baryon densities. Furthermore, a numerical calculation indicates that the model respects causality and the values of the transport coefficients (such as shear viscosity to entropy (η/s) ratio, and the speed of sound etc.) suitably match with the predictions of other HG models. The aim in this paper is to obtain the variations of freeze-out volume in a slice of unit rapidity i.e. dV/dy as well as total volume of the fireball with respect to center-of-mass energy ($\sqrt{S_{NN}}$) and confront our model calculations with the corresponding thermal freeze-out volume obtained from the Hanbury-Brown-Twiss (HBT) pion interferometry. We also test the validity of our model in extracting the total multiplicities as well as the central rapidity densities of various hadrons such as π^+, K^+, p, ϕ, Λ, Ξ^-, Ω^-, $\bar{\Lambda}$ etc. and in getting the rapidity as well as transverse momentum distributions of various particles produced in different heavy-ion collider experiments in order to examine the role of any hydrodynamic flow on them by matching our predictions with the experimental results. Furthermore, we extend our analysis for the production of light nuclei, hypernuclei and their antinuclei over a broad energy range from Alternating Gradient Synchrotron (AGS) to Large Hadron Collider (LHC) energies, for which the experimental data have started appearing.

PACS numbers: 12.38.Mh, 12.38.Gc, 25.75.Nq, 24.10.Pa

---

* corresponding author: *sktiwari4bhu@gmail.com*

I. INTRODUCTION

The ultimate goal of ultra-relativistic heavy-ion collisions is to produce a highly excited and dense matter which possibly involves a phase transition from a hot, dense hadron gas (HG) to a deconfined quark matter called as quark-gluon plasma (QGP) [1-3]. In this state the degrees of freedom are those of quarks and gluons only. One hopes that by colliding heavy nuclei one can create a fireball with an extremely large energy density extending over a sufficiently large space-time volume so that an equilibrated quark-gluon plasma may be formed. However, experimental and theoretical investigations made so far reveal that it is indeed difficult to get an unambiguous evidence for QGP formation. It is very important to understand the dynamics of the collisions in order to suggest any unique signal for QGP. Such information can be obtained by analyzing the properties of various particles which are emitted from various stages of the collisions. The global properties and dynamics of later stages can be best studied via hadronic observables such as hadron yields, ratios, rapidity distributions and transverse mass spectra [4].

In our previous paper henceforth referred as I [5], we have proposed a thermodynamically consistent excluded-volume model and studied different thermodynamical properties of HG such as number density, energy density, pressure etc.. It is indeed surprising that the predictions of our geometrical model regarding the detailed features of various hadron ratios and their variations with respect to the center-of-mass energy ($\sqrt{s_{NN}}$) are successfully tested with the available experimental data upto Relativistic Heavy-Ion Collider (RHIC) energies. We know that if a system passes through a mixed phase in a first order phase transition, then it can possess a much larger space-time extent than what we expect from a system if it remains in the hadronic phase only. Thus the freeze-out volume V of the fireball formed in heavy-ion collisions, is a significant quantity which can give a hint regarding the occurrence of mixed phase during a phase transition. Furthermore, the freeze-out volume throws light on the collective expansion and/or anisotropic flow of the fluid existing in the fireball before a final thermal freeze-out occurs. In this paper, we calculate the variations of chemical freeze-out volumes for π^+, K^+, and K^- with respect to $\sqrt{s_{NN}}$ and compare our predictions with the HBT interferometry data for the thermal freeze-out volume. It gives an independent confirmation pertinent to correctness of the geometrical assumptions involved in our model on the space dynamics of the fireball. We also attempt to show the variations of total multiplicities as well as the multiplicity in a slice of unit rapidity at midrapidity ($y = 0$) for various emitted hadrons, e.g., π^+, K^+, K^-, ϕ, Λ, Ξ^-,Ω^-, and $\bar{\Lambda}$. Further, we extend our model to deduce the rapidity as well as transverse mass spectra of hadrons and compare them with the experimental data available in order to illustrate the role of hydrodynamic flow of the fluid.

In heavy-ion collisions, rapidity densities of produced particles are strongly related to the energy density and/or entropy density created in the collisions [6]. Further, the dependence of transverse mass spectra of hadrons on $\sqrt{s_{NN}}$ can yield insight into the evolution of a radial flow present in the dense fluid formed in the collision [7]. Earlier different types of approaches have been taken into account for studying rapidity distributions and transverse mass spectra [8-13]. Hadronic spectra from purely thermal models usually reveal an isotropic distribution of particles [8] and hence the rapidity spectra obtained with the thermal models do not reproduce the features of the experimental data satisfactorily. Similarly, the transverse mass spectra from the thermal models reveal a more steeper curve than that observed experimentally. The comparisons illustrate that the fireball formed in heavy-ion collisions does not expand isotropically in nature and there is a prominent input of collective flow in the longitudinal and transverse directions which finally causes anisotropy in the rapidity and transverse mass distributions of the hadrons after the freeze-out. A lot of work has been done in recent years on thermal model calculations incorporating the effect of flow [14-23]. Here we mention some kinds of models of thermal and collective flow used in the literature. Hydrodynamical properties of the expanding fireball have been initially discussed by Landau and Bjorken for the stopping and central-rapidity regimes, respectively [9]. However, collisions even at RHIC energies reveal that they are neither fully stopped, nor fully transparent. As the collision energy increases, the longitudinal flow grows stronger and leads to a cylindrical geometry as postulated in Ref. [10-12]. They assume that the fireballs are distributed uniformally in the longitudinal direction and demonstrate that the available data can consistently be described in a thermal model with inputs of chemical equilibrium and flow, although they have used the experimental data for small systems only. They use two simple parameters : transverse flow velocity (β_r) and temperature (T) in their models. In Ref. [13], non-uniform flow model is used to analyze the spectra specially to reproduce the dip at midrapidity in the rapidity spectra of baryons by assuming that the fireballs are distributed non-uniformly in the longitudinal phase space. In Ref. [24-26], the rapidity-dependent baryon chemical potential has been invoked to study the rapidity spectra of hadrons. In certain hydrodynamical models [27,28], measured transverse momentum (p_T) distributions in $Au-Au$ collisions at $\sqrt{s_{NN}} = 130\ GeV$ [29-31] have been described successfully by incorporating a radial flow. In Ref. [32], rapidity spectra of mesons have been studied using viscous relativistic hydrodynamics in a 1+1 dimension assuming a non-boost invariant Bjorken flow in the longitudinal direction. They have also analyzed the effect of the shear viscosity on the longitudinal expansion of the matter. Shear viscosity counteracts the gradients of the velocity field, as a consequence slows down the longitudinal expansion. In this paper, we attempt to calculate the rapidity density of various particles at midrapidity by using our excluded-volume model of HG and we find a good agreement between our model calculations and the experimental data. However, when we calculate the rapidity distributions of various particles, we find that the distribution always takes a narrow shape in comparison to the experimental data and thus indicating that our thermal model alone is not capable to describe the experimental data in forward and backward rapidity regions. In a similar way, the transverse mass spectra of hadrons as obtained in our model again does not describe the experimental data properly. Our analysis clearly necessitates the presence of an additional flow factor to be introduced in the model in order to provide a suitable description of the data.

We plan to study the rapidity distributions and transverse mass spectra of hadrons using our model in I [5] for a hot, dense HG which is based on an excluded-volume approach [33] formulated in a thermodynamically consistent way. We have assigned an equal hard-core size to each type of baryons in the HG while the mesons are treated as pointlike particles. We use the chemical freeze-out criteria to relate the thermal parameters T and μ_B with the collision energies [5]. We further emphasize that we have used this hadronic equation of state (EOS) together with a suitable EOS for QGP in order to obtain the QCD phase diagram and the associated critical point [34]. The plan of the paper runs as follows : the next section is dedicated to the formulation of our model for the study of the rapidity distributions and transverse mass spectra of hadrons using purely thermal source. In the third section, we modify the formula for the rapidity distributions by incorporating a flow velocity in the longitudinal direction and similarly the formula for the transverse mass spectra is also modified by incorporating a collective flow in the longitudinal as well as in the transverse direction. In section IV, we compare the experimental data with our predictions regarding rapidity density, transverse mass spectra and transverse momentum spectra of hadrons at RHIC energies (130 GeV and 200 GeV) and LHC energy (2.76 TeV). We have also shown the rapidity spectra of π^- at Super Proton Synchrotron (SPS) energies. As $\sqrt{s_{NN}}$ increases, the longitudinal as well as the transverse flow also increase which means that the experiments will observe a larger amount of collective flow at LHC. We have also deduced total mean multiplicities, mid-rapidity yields of various hadrons and their rapidity densities and studied their variations with $\sqrt{s_{NN}}$. Thus we determine the freeze-out volume and/or dV/dy in order to ascertain whether the emissions of all hadrons occur from the same hypersurface of the fireball. We also analyze the experimental data on the production of light nuclei, hypernuclei and their antiparticles over a broad energy going from AGS to RHIC energies. This analysis thus fully demonstrates the validity of our EOS in describing all the features of a hot, dense HG. Finally, in the last section we succinctly give the conclusions and summary.

II. HADRONIC SPECTRA WITH THE THERMAL SOURCE

A. Rapidity Distributions

To study the rapidity distributions and transverse mass spectra of the hadrons, we extend excluded-volume model as proposed in I [5], which was found to describe the hadron ratios and yields at various $\sqrt{s_{NN}}$ from lower AGS energies upto RHIC energies with remarkable success. We have incorporated the excluded-volume correction directly in the grand canonical partition function of HG in a thermodynamically consistent manner. We obtain the number density n_i^{ex} for ith species of baryons after excluded-volume correction as follows [5]:

$$n_i^{ex} = (1-R)I_i\lambda_i - I_i\lambda_i^2\frac{\partial R}{\partial \lambda_i} + \lambda_i^2(1-R)I_i^{'}, \qquad (1)$$

where $R = \sum_i n_i^{ex}V_i^0$ is the fractional occupied volume by the baryons [5,34]. $V_i^0 = 4\pi\ r^3/3$ is the eigen-volume of each baryon having a hard-core radius r and λ_i is the fugacity of ith baryon. Further, I_i is the integral of the baryon distribution function over the momentum space [5].

We can rewrite Eq. (1) in the following manner :

$$
\begin{aligned}
n_i^{ex} = \frac{g_i \lambda_i}{(2\pi)^3} \Bigg[\left((1-R) - \lambda_i \frac{\partial R}{\partial \lambda_i} \right) \int_0^\infty \frac{d^3k}{\left[exp\left(\frac{E_i}{T}\right) + \lambda_i \right]} \\
-\lambda_i (1-R) \int_0^\infty \frac{d^3k}{\left[exp\left(\frac{E_i}{T}\right) + \lambda_i \right]^2} \Bigg].
\end{aligned} \tag{2}
$$

This reveals that the invariant distributions are [10,11] :

$$
\begin{aligned}
E_i \frac{d^3N_i}{dk^3} = \frac{g_i V \lambda_i}{(2\pi)^3} \Bigg[\left((1-R) - \lambda_i \frac{\partial R}{\partial \lambda_i} \right) \frac{E_i}{\left[exp\left(\frac{E_i}{T}\right) + \lambda_i \right]} \\
-\lambda_i (1-R) \frac{E_i}{\left[exp\left(\frac{E_i}{T}\right) + \lambda_i \right]^2} \Bigg].
\end{aligned} \tag{3}
$$

Using :

$$
E_i \frac{d^3N_i}{dk^3} = \frac{dN_i}{dy \; m_T \; dm_T \; d\phi}, \tag{4}
$$

we get :

$$
\begin{aligned}
\frac{dN_i}{dy \; m_T \; dm_T \; d\phi} = \frac{g_i V \lambda_i}{(2\pi)^3} \Bigg[\left((1-R) - \lambda_i \frac{\partial R}{\partial \lambda_i} \right) \frac{E_i}{\left[exp\left(\frac{E_i}{T}\right) + \lambda_i \right]} \\
-\lambda_i (1-R) \frac{E_i}{\left[exp\left(\frac{E_i}{T}\right) + \lambda_i \right]^2} \Bigg],
\end{aligned} \tag{5}
$$

Here y is the rapidity variable and transverse mass $m_T = \sqrt{m^2 + {p_T}^2}$. Also E_i is the energy of ith baryon and V is the total volume of the fireball formed at chemical freeze-out and N_i is the total number of ith baryons. We assume that the freeze-out volume of the fireball for all types of hadrons at the time of the homogeneous emissions of hadrons remains the same.

By inserting $E_i = m_T \; coshy$ in Eq. (5) and integrating the whole expression over transverse component we can get the rapidity distributions of baryons as follows:

$$\left(\frac{dN_i}{dy}\right)_{th} = \frac{g_i V \lambda_i}{(2\pi^2)} \Bigg[\left((1-R) - \lambda_i \frac{\partial R}{\partial \lambda_i}\right) \int_0^\infty \frac{m_T^2\ coshy\ dm_T}{\left[exp\left(\frac{m_T\ coshy}{T}\right) + \lambda_i\right]} \\ -\lambda_i (1-R) \int_0^\infty \frac{m_T^2\ coshy\ dm_T}{\left[exp\left(\frac{m_T\ coshy}{T}\right) + \lambda_i\right]^2}\Bigg]. \tag{6}$$

Eq.(6) gives the rapidity distributions of baryons arising due to a stationary thermal source. Here we evaluate the rapidity distributions of hadrons at $p_T = 0$ as the data have been taken for the $p_T = 0$ case.

Similarly, the rapidity density of mesons can be had by using the following formula :

$$\left(\frac{dN_m}{dy}\right)_{th} = \frac{g_m V \lambda_m}{(2\pi^2)} \int_0^\infty \frac{m_T^2\ coshy\ dm_T}{\left[exp\left(\frac{m_T\ coshy}{T}\right) - \lambda_m\right]}. \tag{7}$$

Here g_m, λ_m are the degeneracy factor and fugacity of the meson m, respectively.

B. Transverse Mass Spectra

We use Boltzmann statistics in deriving formula for the transverse mass spectra because we want to calculate spectra of hadrons only at RHIC energies, where the effect of quantum statistics is found to be negligible [10]. In the Boltzmann's approximation, Eq.(5) can be reduced to a simple form :

$$\frac{dN_i}{dy\ m_T\ dm_T\ d\phi} = \frac{g_i V \lambda_i}{(2\pi)^3} \left[\left((1-R) - \lambda_i \frac{\partial R}{\partial \lambda_i}\right)\right] E_i \left[exp\left(\frac{-E_i}{T}\right)\right]. \tag{8}$$

Putting $E_i = m_T\ coshy$ in Eq.(8) and integrating over rapidity (y) we get the transverse mass spectra as follows :

$$\frac{dN_i}{m_T\ dm_T} = \frac{g_i V \lambda_i}{(2\pi)^3} \left[(1-R) - \lambda_i \frac{\partial R}{\partial \lambda_i}\right] \int_0^\infty m_T\ coshy \left[exp\left(\frac{-m_T\ coshy}{T}\right)\right] dy d\phi, \tag{9}$$

or, this means :

$$\frac{dN_i}{m_T\ dm_T} = \frac{g_i V \lambda_i}{(2\pi^2)} \left[(1-R) - \lambda_i \frac{\partial R}{\partial \lambda_i}\right] m_T\ K_1\left(\frac{m_T}{T}\right), \tag{10}$$

where $K_1\Big(\dfrac{m_T}{T}\Big)$ is the modified Bessel's function and is given by the following expression :

$$K_1\Big(\frac{m_T}{T}\Big) = \int_0^{\infty} coshy \,\Big[exp\,\Big(\frac{-m_T\; coshy}{T}\Big)\Big]dy. \tag{11}$$

Similarly transverse mass spectrum of mesons can be evaluated as follows :

$$\frac{dN_m}{m_T\; dm_T} = \frac{g_m V \lambda_m}{(2\pi^2)}\; m_T\; K_1\Big(\frac{m_T}{T}\Big). \tag{12}$$

III. HADRONIC SPECTRA WITH THE EFFECT OF FLOW

In the previous section, we have obtained the expression for rapidity distributions as well as transverse mass spectra arising from a stationary thermal source only. In this section, we modify the expression for rapidity spectra i.e. Eq. (6), by incorporating a flow velocity to a stationary thermal system in the longitudinal direction and thus we attempt to explain the experimental data in the full rapidity region. The resulting rapidity spectrum of ith hadron, after the incorporation of the flow velocity in the longitudinal direction is [10,11]:

$$\frac{dN_i}{dy} = \int_{-\eta_{max.}}^{\eta_{max.}} \Big(\frac{dN_i}{dy}\Big)_{th}(y-\eta)\; d\eta, \tag{13}$$

where $\Big(\dfrac{dN_i}{dy}\Big)_{th}$ can be calculated by using Eq.(6) for the baryons and by Eq.(7) for the mesons. The average longitudinal velocity is [13,35]:

$$\langle\beta_L\rangle = tanh\Big(\frac{\eta_{max.}}{2}\Big). \tag{14}$$

Here $\eta_{max.}$ is an important parameter which provides the upper rapidity limit for the longitudinal flow velocity at particular $\sqrt{s_{NN}}$ and it's value is determined by the best experimental fit. The value of $\eta_{max.}$ increases with the increasing $\sqrt{s_{NN}}$ and hence β_L also increases.

In the case of transverse mass spectra, we incorporate flow velocity in both the directions, longitudinal as well as transverse directions in order to describe the experimental data satisfactorily. However, we assume radial type of flow velocity in the transverse direction which imparts a radial velocity boost on top of the thermal distribution. We define the four velocity field in both the directions as follows [36] :

$$u^{\mu}(\rho,\eta) = (cosh\rho\ cosh\eta, \bar{e_r}\ sinh\rho, cosh\rho\ sinh\eta), \tag{15}$$

where ρ is the radial flow velocity in the transverse direction and η is the flow velocity in the longitudinal direction. Once we have defined the flow velocity field, we can calculate the invariant momentum spectrum by using the following formula [10,37] :

$$E_i\ \frac{d^3N_i}{dk^3} = \frac{g_iV\lambda_i}{(2\pi)^3}\ \Big[(1-R) - \lambda_i\frac{\partial R}{\partial\lambda_i}\Big] \int exp\Big(\frac{-k_{\mu}u^{\mu}}{T}\Big)\ k_{\lambda}\ d\sigma_{\lambda}. \tag{16}$$

In the derivation of Eq.(16) we assume that an isotropic thermal distribution of hadrons is boosted by the local fluid velocity u^{μ}. Now the resulting spectrum can be written as follows [10] :

$$\begin{aligned}\frac{dN_i}{m_T\ dm_T\ dy} &= \frac{g_iV\lambda_i\ m_T}{(2\pi)^3}\ \Big[(1-R) - \lambda_i\frac{\partial R}{\partial\lambda_i}\Big] \int r\ dr\ d\phi\ d\zeta \\ &\times exp\Big(- \frac{m_Tcosh(y-\eta)\ cosh\rho - p_Tsinh\rho\ cos\phi}{T}\Big).\end{aligned} \tag{17}$$

The freeze-out hypersurface $d\sigma_{\lambda}$ in Eq.(16) is parametrized in cylindrical coordinates (r,ϕ,ζ), where the radius r can lie between 0 and R i.e. the radius of the fireball at freeze-out, the azimuthal angle ϕ lies between 0 and 2π, and the longitudinal space-time rapidity variable ζ varies between $-\eta_{max.}$ and $\eta_{max.}$. Now, integrating Eq.(17) over ϕ as well as ζ, we get the final expression for the transverse mass spectra [10] :

$$\frac{dN_i}{m_Tdm_T} = \frac{g_iV\lambda_i\ m_T}{(2\pi^2)}\ \Big[(1-R) - \lambda_i\frac{\partial R}{\partial\lambda_i}\Big] \int_0^R r\ dr\ K_1\Big(\frac{m_T\ cosh\rho}{T}\Big)I_0\Big(\frac{p_T\ sinh\rho}{T}\Big). \tag{18}$$

Here $I_0\Big(\frac{p_T\ sinh\rho}{T}\Big)$ is the modified Bessel's function given by :

$$I_0\Big(\frac{p_T\ sinh\rho}{T}\Big) = \frac{1}{2\pi}\int_0^{2\pi} exp\Big(\frac{p_T\ sinh\rho\ cos\phi}{T}\Big)d\phi, \tag{19}$$

where ρ is given by $\rho = tanh^{-1}\beta_r$, with the velocity profile chosen as $\beta_r = \beta_s\ \Big(\xi\Big)^n$ [10,11]. β_s is the maximum surface velocity and is treated as a free parameter and $\xi = \Big(r/R\Big)$. The average of the transverse velocity can be evaluated as [31]:

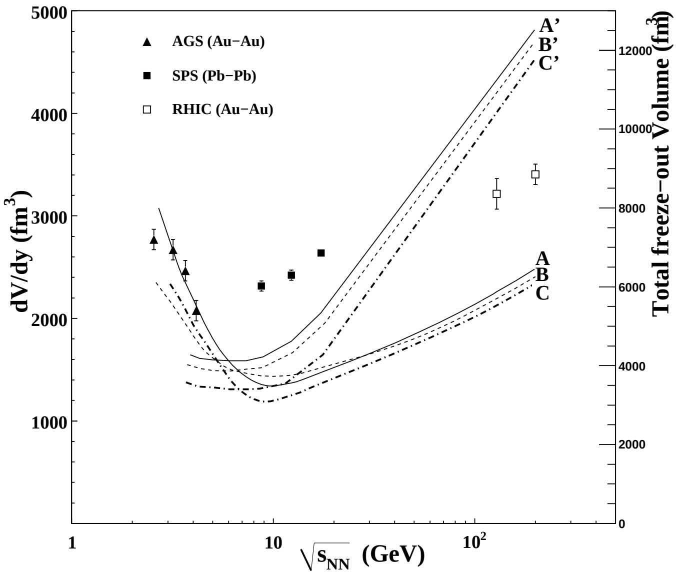

FIG. 1: Energy dependence of the freeze-out volume for the central nucleus-nucleus collisions. The symbols are the HBT data for freeze-out volume V_{HBT} for the π^+ [38]. A' ,B' and C' are the total freeze-out volume and A ,B and C depict the dV/dy as found in our model for π^+, K^+ and K^- , respectively.

$$< \beta_T >= \frac{\int \beta_s \xi^n \xi \; d\xi}{\int \xi \; d\xi} = \Big(\frac{2}{2+n}\Big)\beta_s. \tag{20}$$

In our calculation we use a linear velocity profile, $n = 1$ and R is the maximum radius of the expanding source at freeze-out $(0 < \xi < 1)$ [31]. Similarly following equation can be used to calculate transverse mass spectra for mesons :

$$\frac{dN_m}{m_T dm_T} = \frac{g_m V \lambda_m \; m_T}{(2\pi^2)} \int_0^R r \; dr \; K_1\Big(\frac{m_T \; cosh\rho}{T}\Big) I_0\Big(\frac{p_T \; sinh\rho}{T}\Big). \tag{21}$$

IV. RESULTS AND DISCUSSIONS

We have used freeze-out temperature and baryon chemical potential as determined by fitting the particle ratios as described in I [5]. Then we use suitable parametrizations for T and μ_B in terms of center-of-mass energies. We have used hard-core radius $r = 0.8 \; fm$ for all types of baryons. We have considered all the particles and the resonances upto mass of

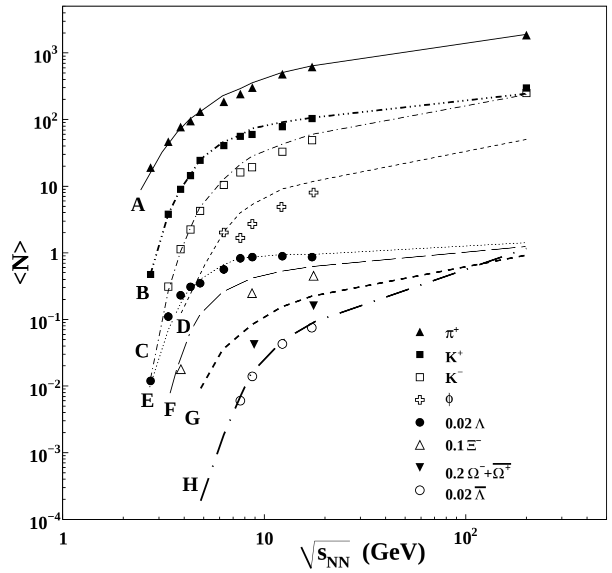

FIG. 2: Variations of total multiplicities of π^+, K^+, K^-, ϕ, Λ, Ξ^-, $(\Omega^- + \bar{\Omega}^+)$, and $\bar{\Lambda}$ with respect to center-of-mass energy predicted by our model. Experimental data measured in central $Au - Au/Pb - Pb$ collisions [39-55] have also been shown for comparison. In this figure, A, B, C, D, E, F, G, and H represent the multiplicities of π^+, K^+, K^-, ϕ, Λ, Ξ^-, $(\Omega^- + \bar{\Omega}^+)$, and $\bar{\Lambda}$, respectively.

2 GeV/c^2 in our calculation. We have used resonances having well defined masses, widths etc. and branching ratios for sequential decays are also suitably incorporated.

Although the emission of hadrons from a statistical thermal model essentially invokes the idea of equilibration, it does not reveal any information regarding the existence of a QGP phase before hadronization. However, if the constituents of the fireball have gone through a mixed phase, volume V of the fireball at freeze-out is expected to be much larger than what we expect from a system if it remains throughout in the hadronic phase only. In Fig. 1, we have shown V and dV/dy as obtained in our excluded-volume model and their variations with the center-of-mass energy. For this purpose, we have used the data for total multiplicities of π^+, K^+, K^- and after dividing with their corresponding number densities obtained in our model, we get V for π^+, K^+, and K^-, respectively. Similarly for deducing dV/dy, we use the data for dN/dy and divide by the corresponding number density. We have compared predictions of our model with the experimental data obtained from the pion

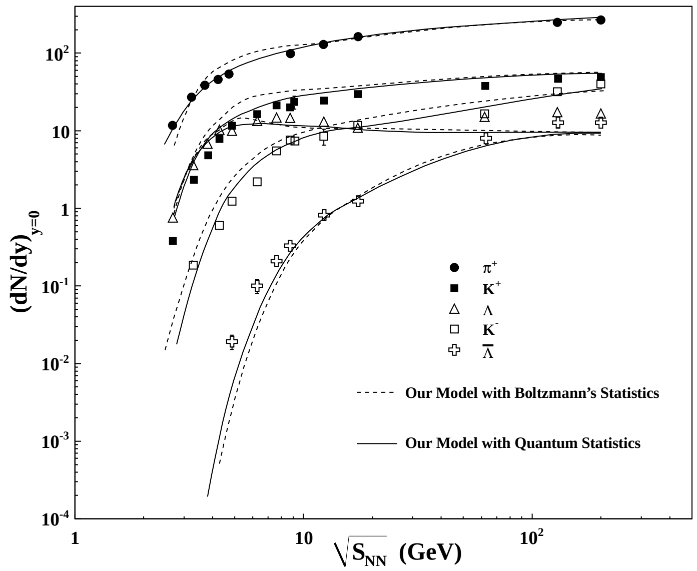

FIG. 3: Variation of rapidity distributions of various hadrons with respect to $\sqrt{s_{NN}}$ at midrapidity. Lines show our model calculation. Symbols are the experimental data [7,56,57].

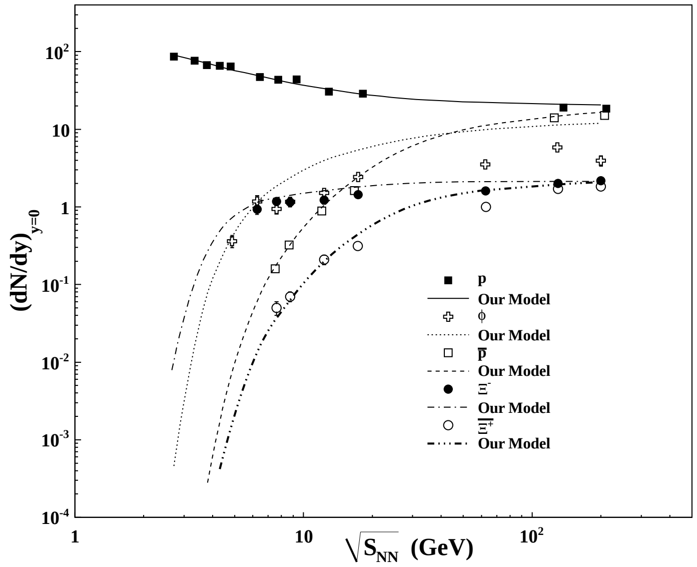

FIG. 4: Energy dependence of rapidity distributions of hadronic species at midrapidity ($y = 0$) for central nucleus-nucleus collisions. Lines are the model calculations and symbols are the experimental results [7,56,57] at various $\sqrt{s_{NN}}$.

interferometry (HBT) [38] which in fact reveal thermal (kinetic) freeze-out volume. Our results support the finding that the decoupling of strange mesons from the fireball takes place earlier than the π-mesons. Moreover, a flat minimum occurs in the curves around energy $\approx 8\ GeV$, then the volume rapidly increases. At RHIC energy, the volume of the fireball is around 12000 fm^3 which is much larger than the volume of gold nucleus used in the collisions.

In order to calculate total multiplicities of hadrons, we first determine the total freeze-out volume for K^+ by dividing the experimentally measured multiplicities of K^+ at different center-of-mass energies with it's number density as calculated in our model at different center-of-mass energies. We assume that the fireball after expansion, achieves the stage of chemical equilibrium and the freeze-out volume of the fireball for all types of hadrons at the time of the homogeneous emissions of hadrons remains same for all particles. This freeze-out volume thus extracted for K^+, has been used to calculate multiplicities of all other hadrons from corresponding number densities at different $\sqrt{s_{NN}}$. Figure 2 shows the center-of-mass energy dependence of multiplicities of hadrons π^+, K^+, K^-, ϕ, Λ, Ξ^-, $(\Omega^- + \bar{\Omega^+})$, and $\bar{\Lambda}$ as predicted by our model calculation. We also show here corresponding experimental data measured in central $Au-Au/Pb-Pb$ collisions [39-55] for comparison. We observe an excellent agreement between our model calculation and experimental data for the total multiplicities of all particles except ϕ, Ξ^-, and Ω^-, where we see small deviations. Again, the thermal multiplicities for all these particles are larger than the experimental values. This analysis again suggests a new and different mechanisms for the production of these particles.

In Fig.3, we compare the experimental midrapidity data [7,56,57] of various hadron species over a broad energy range from AGS to RHIC energies with the results of our model calculations. We use the same freeze-out volume of the fireball for each hadron as extracted for K^+ in our model calculation. We also show the comparison between the results calculated using our model with the Boltzmann's statistics, as used in our previous paper [58], with the results calculated with full quantum statistics. As expected, both results differ only at lower energies. However, the results with quantum statistics give much closer agreement with the experimental data. Figure 4 shows the energy dependence of midrapidity distributions of various hadrons like p, ϕ, $\bar{p}$, Ξ^-, and $\bar{\Xi^+}$. We observe that the results obtained in our model show a close agreement with the experimental data [7,56,57]. However, our model calculation again differs at higher energies for multistrange particles in comparison

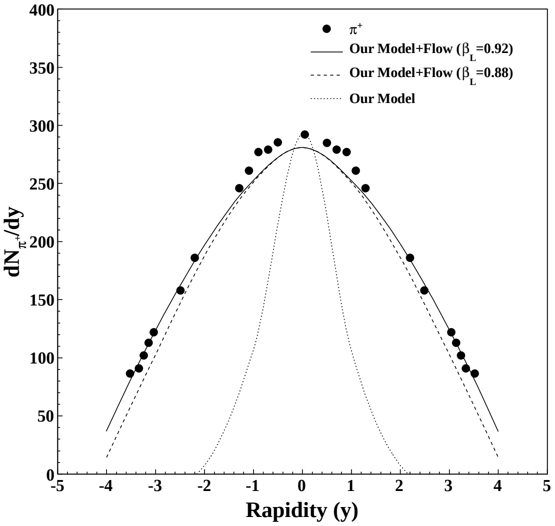

FIG. 5: Rapidity distribution of π^+ at $\sqrt{s_{NN}} = 200 GeV$. Dotted line shows the rapidity distribution calculated in our thermal model. Solid line and dashed line show the results obtained after incorporating longitudinal flow in our thermal model. Symbols are the experimental data [59].

to experimental data, which appears to be a common problem of all thermal models.

In Fig.5, we present the rapidity distribution of π^+ for central $Au + Au$ collisions at $\sqrt{s_{NN}} = 200\ GeV$ over full rapidity range. Dotted line shows the distribution of π^+ due to stationary thermal source which describes only the midrapidity data while it fails to describe the experimental data at other rapidities. Solid line shows the rapidity distributions of π^+ after incorporation of longitudinal flow in our thermal model and again in a good agreement with the experimental data [59]. After fitting the experimental data, we get the value of $\eta_{max.} = 3.20$ and hence the longitudinal flow velocity $\beta_L = 0.922$ at $\sqrt{s_{NN}} = 200\ GeV$. For comparison and testing the appropriateness of parameter, we also show the rapidity distributions at different values of the parameter, $\eta_{max.} = 2.80$ i.e. $\beta_L = 0.88$, which is shown by the dashed line in the figure. We find that the results now differ.

In Fig.6, we analyze the experimental data [60] on rapidity distributions of π^- at various $\sqrt{s_{NN}}$ in terms of our model calculation to constrain the allowed distribution of the longitudinal velocities of the fluid elements. We find that our model results are in good agreement with the experimental data at these energies. Figure 7 demonstrates the variation of longitudinal flow velocities extracted in our model with respect to $\sqrt{s_{NN}}$ and it shows that the longitudinal flow velocity increases with the increasing $\sqrt{s_{NN}}$. We compare our results with

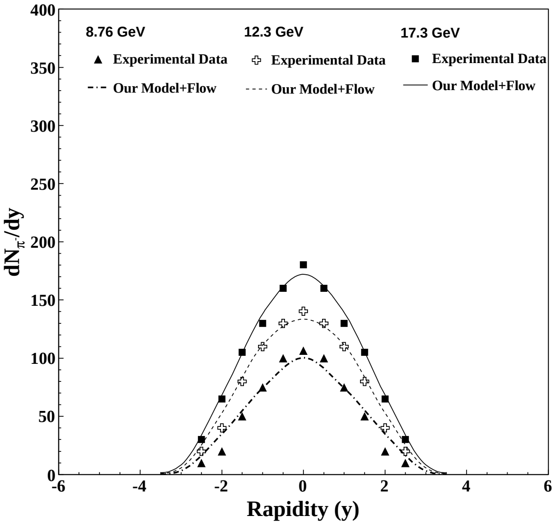

FIG. 6: Rapidity distribution of π^- at $\sqrt{s_{NN}} = 8.76\ GeV, 12.3\ GeV$ and $17.3\ GeV$. Lines are our model calculation and symbols are experimental data [60].

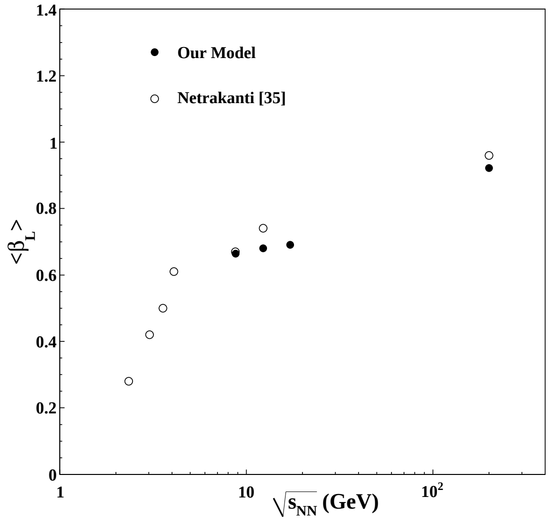

FIG. 7: Variations of the longitudinal flow velocities with respect to $\sqrt{s_{NN}}$. Open circles are the results of Ref.[35].

that calculated in Ref.[35] and find that a slight difference exists between these two results.

Figures 8 and 9 demonstrate the rapidity distributions of proton and anti-proton, respectively at $\sqrt{s_{NN}} = 200\ GeV$. Again, our curves describe successfull the experimental data [61]. Similarly in Figures 10 and 11 we show the rapidity distributions for K^+ and K^-,

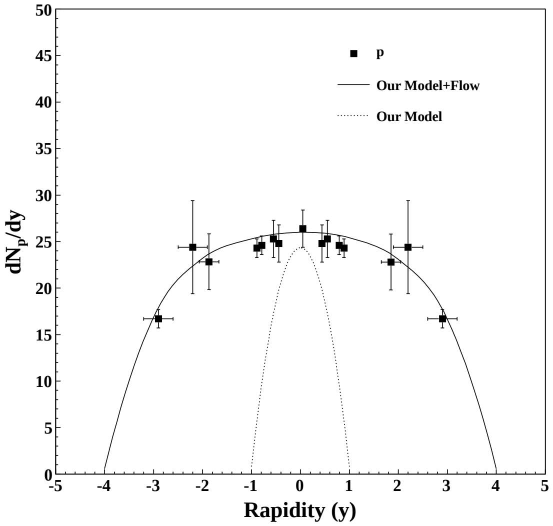

FIG. 8: Rapidity distribution of proton for central $Au - Au$ collisions at $\sqrt{s_{NN}} = 200\ GeV$. Dotted line shows the rapidity distribution due to purely thermal source and solid line shows the result after incorporating the longitudinal flow velocity in our thermal model. Symbols are the experimental data [61].

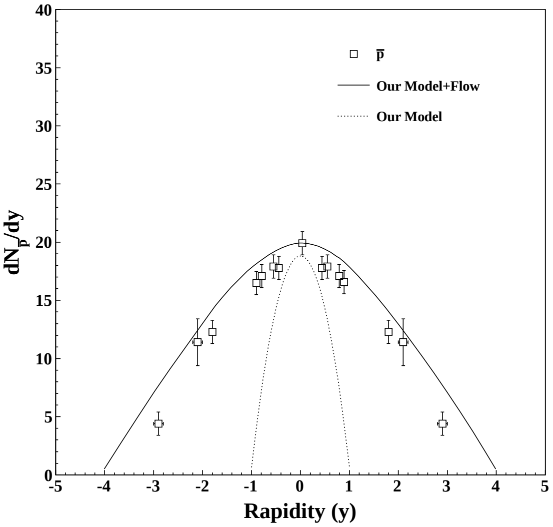

FIG. 9: Rapidity distribution of anti-proton for central $Au - Au$ collisions at $\sqrt{s_{NN}} = 200\ GeV$. Dotted line shows the rapidity distribution due to purely thermal source and solid line shows the result after incorporating the longitudinal flow in our thermal model. Symbols are the experimental data [61].

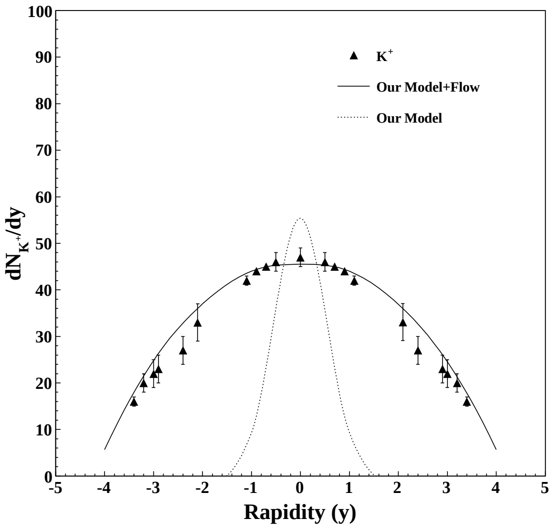

FIG. 10: Rapidity distribution of K^+ at $\sqrt{s_{NN}} = 200\ GeV$. Dotted line shows the rapidity distribution due to purely thermal source and solid line shows the result after incorporating longitudinal flow in the thermal model. Symbols are the experimental data [62].

respectively at $\sqrt{s_{NN}} = 200\ GeV$. We have used the same value of parameter β_L and V for each particle.

Figure 12 shows the analysis of the transverse mass spectra of π^+ and proton for the most central collisions of $Au - Au$ at $\sqrt{s_{NN}} = 130\ GeV$ in terms of our model calculation. We have neglected the contributions from resonance decays in our calculations here because the contributions from resonance decays affect the transverse mass spectra only at the lower transverse mass side i.e. $m_T < 0.3\ GeV$. So, our model calculation show some difference with the experimental data [31] for $m_T < 0.3\ GeV$ but there is a good agreement between our model calculation and experimental results for $m_T > 0.3\ GeV$. We also show our model results for π^+ at different values of β_s just for comparison. Similarly Figure 13 shows the transverse mass spectra of K^+ and ϕ for the most central collisions of $Au - Au$ at $\sqrt{s_{NN}} = 130\ GeV$. Our calculation is quite successfull in describing the experimental data [31,64]. However, our model fails again in the case of multistrange particle ϕ. We need to devise some different mechanism to explain the experimental results for multistrange particles. By fitting the experimental results, we get the value of $\beta_s = 0.45$ and hence transverse flow velocity $\beta_r = 0.30$ at $\sqrt{s_{NN}} = 130\ GeV$, and is less than that extracted in Ref.[31]. It may be due to different freeze-out temperature used in our model.

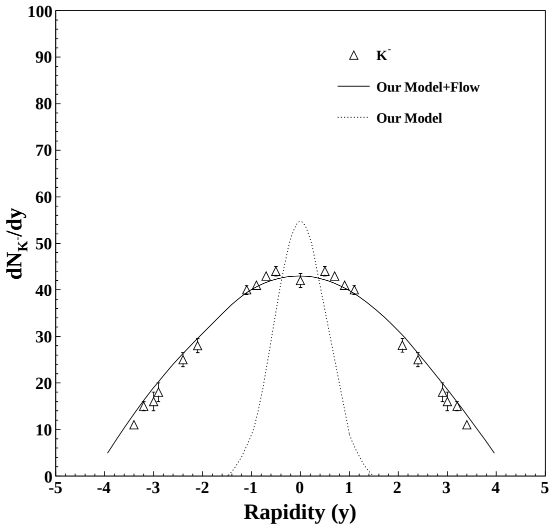

FIG. 11: Rapidity distribution of K^- at $\sqrt{s_{NN}} = 200GeV$. Dotted line shows the rapidity distribution due to purely thermal source and solid line shows the result after incorporating longitudinal flow in our thermal model. Symbols are the experimental data [63].

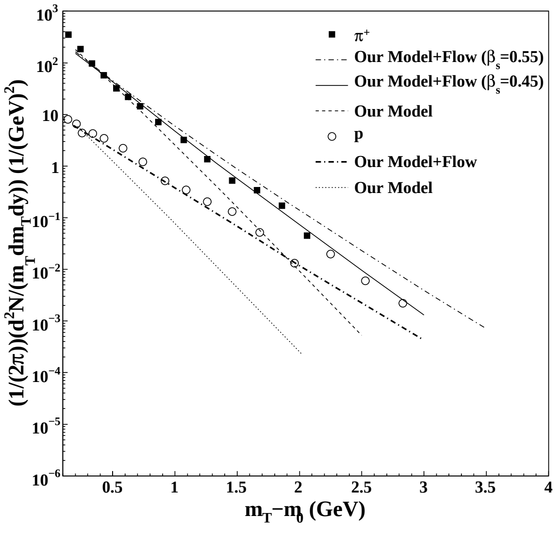

FIG. 12: Transverse mass spectra for π^+ and proton for the most central collision at $\sqrt{s_{NN}} = 130GeV$. Dashed and dotted lines are the results of transverse mass spectra, calculated in our thermal model, for π^+ and proton, respectively. Solid and dash-dotted lines are the results for π^+ and proton, respectively, obtained after incorporation of flow in our thermal model. Symbols are the experimental data [31].

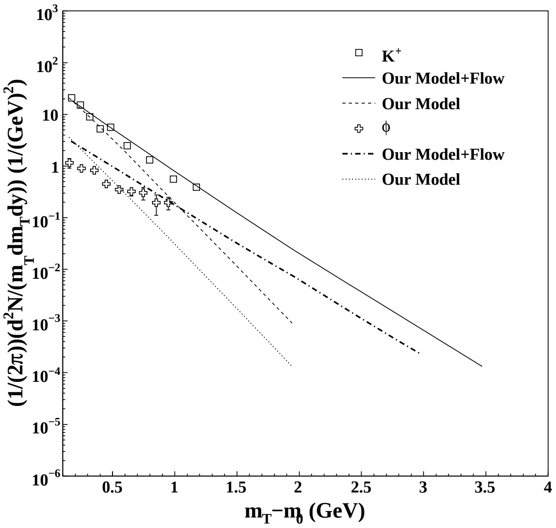

FIG. 13: Transverse mass spectra for K^+ and ϕ for the most central collision at $\sqrt{s_{NN}} = 130\ GeV$. Dashed and dotted lines are the results of transverse mass spectra, calculated in our thermal model, for K^+ and ϕ, respectively. Solid and dash-dotted lines are the results for π^+ and proton, respectively, obtained after incorporation of flow in thermal model. Symbols are the experimental data [31,64].

In Fig. 14, we show the transverse mass spectra of π^+ and proton for the most central collisions of $Au + Au$ at $\sqrt{s_{NN}} = 200\ GeV$. From this figure it is clear that the spectra due to stationary thermal source do not satisfy the experimental data [63] at higher m_T while the thermal source with collective flow can describe the experimental data very well. For comparison, we also show the transverse mass spectra for π^+ at different β_s. In Fig. 15, we present the transverse-mass spectra for K^+ and ϕ at $\sqrt{s_{NN}} = 200\ GeV$. Lines are our model calculations and the symbols represent the experimental data [63,64]. Again, our model fails to describe the experimental data for ϕ at lower m_T. At this $\sqrt{s_{NN}}$ the value of β_s, after best fitting, comes out to be 0.50 and hence transverse flow velocity $\beta_r = 0.33$. The transverse flow velocity is able to reproduce the transverse mass spectra of almost all the hadrons at $\sqrt{s_{NN}} = 200\ GeV$. We also see that the transverse flow velocity increases with the increasing $\sqrt{s_{NN}}$.

We also present the p_T- spectra of hadrons at various center-of-mass energies. In Fig. 16, we show the (p_T) spectra of π^+, K^+ and p for the most central collisions of $Au - Au$

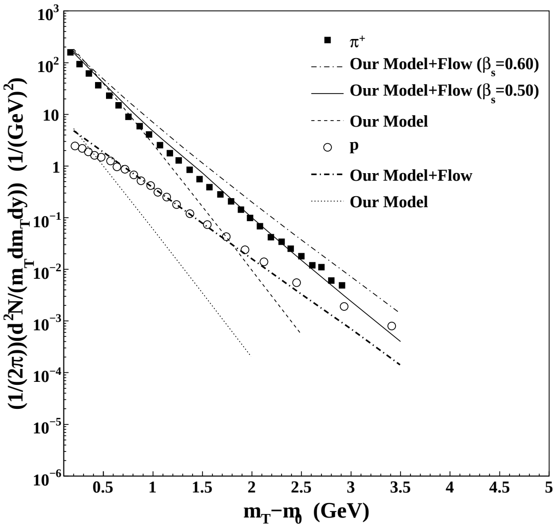

FIG. 14: Transverse mass spectra for π^+ and proton for the most central collisions at $\sqrt{s_{NN}} = 200\ GeV$. Dashed and dotted lines are the transverse mass spectra due to purely thermal source for π^+ and proton, respectively. Solid and dash-dotted lines are the results for π^+ and proton, respectively obtained after incorporation of flow in thermal model. Symbols are the experimental data [63].

at $\sqrt{s_{NN}} = 200\ GeV$. Our model calculations are in close agreement with the experimental data [63]. In Fig. 17, we show the p_T spectra of π^-, K^- and $\bar{p}$ for the $Pb - Pb$ collisions at $\sqrt{s_{NN}} = 2.76\ TeV$ at LHC. Our model calculations give a good fit of the experimental results [65]. We also compare our results for $\bar{p}$ spectrum with the hydrodynamical model [66], which explains successfully the π^-, and K^- spectra but strongly fails to describe the $\bar{p}$ spectrum. We find that our model results are closer with the experimental data than that of Ref.[66]. In Ref. [66], Shen *et al.* have employed $2 + 1$-dimensional viscous hydrodynamics with the lattice QCD-based EOS. They use Cooper-Frye prescription to implement kinetic freeze-out by converting the hydrodynamic output to particle spectra. Due to lack of a proper theoretical and phenomenological knowledge, they use the same parameters for $Pb - Pb$ collisions at LHC energy, which was used for $Au - Au$ collisions at $\sqrt{s_{NN}} = 200\ GeV$. Furthermore, they use the temperature independent η/s ratio in their calculation. After fitting the experimental data, we get $\beta_s = 0.80$ and hence $\beta_r = 0.53$ at this energy which indicates that the collective flow is stronger at this energy than that observed at RHIC

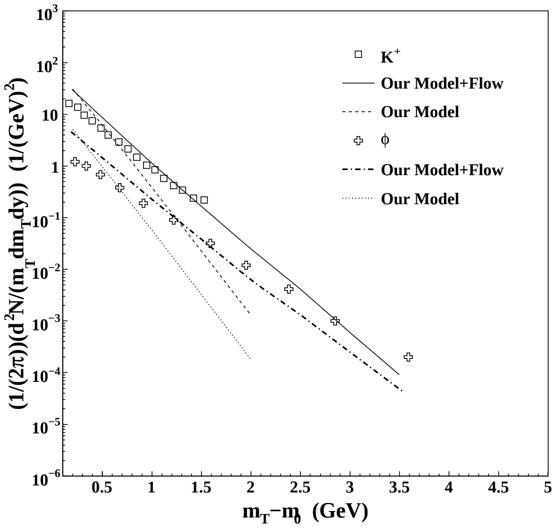

FIG. 15: Transverse mass spectra for K^+ and ϕ for the most central collision at $\sqrt{s_{NN}} = 200 GeV$. Dashed and dotted lines are the transverse mass spectra due to purely thermal source for K^+ and ϕ, respectively. Solid and dash-dotted lines are the results for K^+ and ϕ, respectively, obtained after incorporation of flow in thermal model. Symbols are the experimental data [63,64].

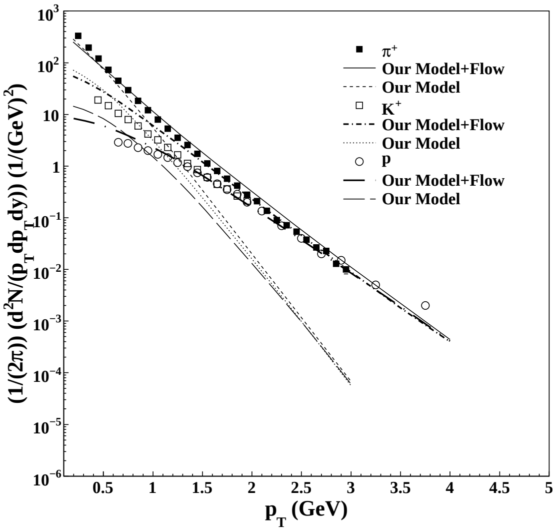

FIG. 16: Transverse momentum spectra for π^+, p, and K^+ for the most central $Au-Au$ collision at $\sqrt{s_{NN}} = 200 GeV$. Lines are the results of our model calculation and symbols are the experimental results [63].

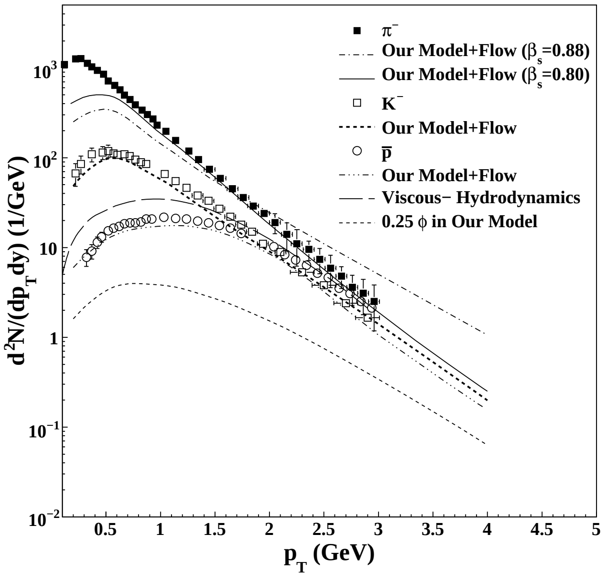

FIG. 17: Transverse momentum spectra of various hadrons for the most central collisions of $Pb-Pb$ at $\sqrt{s_{NN}} = 2.76\ TeV$ from LHC. Lines are the results of model calculations and symbols are the experimental results [65]. Thick-dashed line is the prediction of viscous-hydrodynamical model [66] for $\bar{p}$. Dashed line is the prediction of our model calculation for ϕ meson.

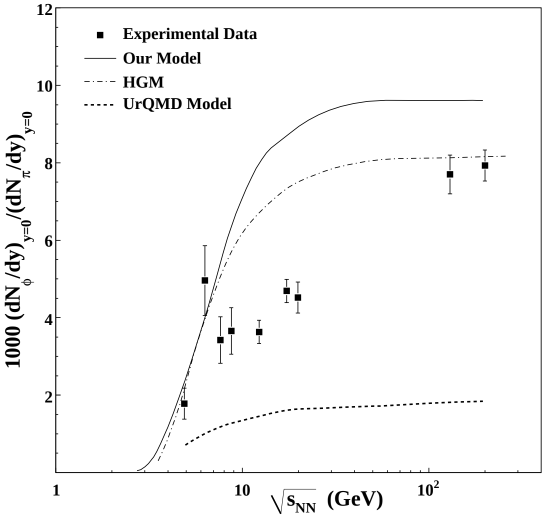

FIG. 18: Energy dependence of the ϕ/π, ($\pi = 1.5(\pi^+ + \pi^-)$) ratio at midrapidity. Dash-dotted line is the result of statistical hadron gas model (HGM) [67]. Solid line represents our model calculation and dashed line is the result of UrQMD model [68]. Symbols are the experimental data points [7].

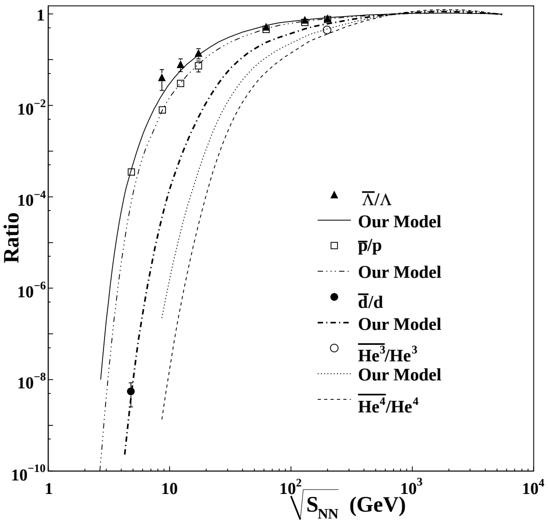

FIG. 19: The energy dependence of anti-baryon to baryon yield and antinuclides to nuclides ratios. Lines are our model calculation and symbols represent the experimental data [74].

energies. We also predict the p_T spectra for ϕ meson at this energy. For comparison, we also show the spectra at different values of parameter $\beta_s = 0.88$.

In order to emphasize how our thermal model fails for multistrange particles, we show in Fig. 18 the variations of the ϕ/π, $(\pi = 1.5(\pi^+ + \pi^-))$ ratio at midrapidity with $\sqrt{s_{NN}}$. We compare our results with the experimental data [7] and statistical hadron gas model (HGM) [67]. We find that our model provides a good description of the experimental data at lower energies but fails to describe the data at higher energies. HGM model, which has included the strangeness saturation factor γ_s to account for the partial equilibration of strangeness, describes the data well at the lower and upper energies while it completely disagrees with the experimental data at the intermediate energies. We also show the results of the hadronic transport model Ultra-relativistic Quantum Molecular Dynamical (UrQMD) [68] in which kaon coalescence mechanism is used for the production of ϕ. The predictions of UrQMD lie well below the experimental data at all energies which suggests that this mechanism fails badly in explaining the production mechanism of ϕ.

We present an analysis of light nuclei, hypernuclei and their anti-particles using the chemical freeze-out concept within our model calculation. The productions of light nuclei and hypernuclei at chemical freeze-out points may not be appropriately calculated, because their binding energies are of the order of few MeV and the chemical freeze-out temperatures

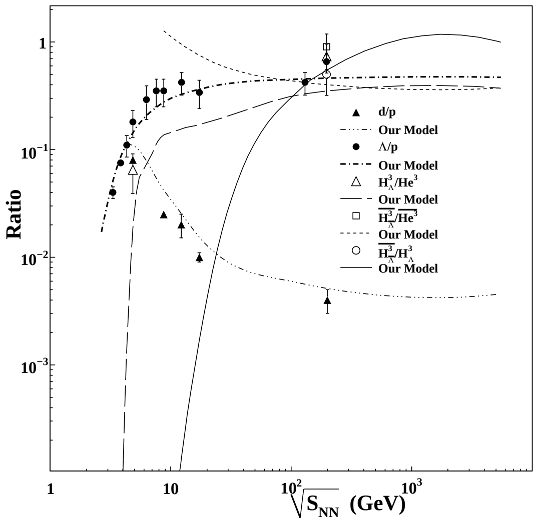

FIG. 20: The energy dependence of various baryons, antibaryons, nuclei, and antinuclei yield ratios. Lines are our model calculation and symbols represent the experimental results [74].

are around $100 - 165\ MeV$. But we know that the relative yield of particles composed of nucleons is mainly determined by the entropy per baryon which is fixed at chemical freeze-out line in our model [5]. This was first outlined in [69] and was subsequently emphasized in [70]. This constitutes the basis of thermal analyses for the yields of light nuclei [71,72]. Thus the production yields of light nuclei and hypernuclei is entirely governed by the entropy conservation. Recently the first measurement of the lightest (anti) hypernuclei was done by the STAR experiment at RHIC [73]. We want to ask an interesting question whether the productions of antinuclei can also be explained by our model. In this paper, we predict and throw light on the production yields of light nuclei, hypernuclei, and heavy baryons (anti-baryons) within our thermal model approach and we compare our thermal model calculations with the experimental data. The thermal freeze-out parameters for these yields are also taken as the same as used for other ratios.

In Fig. 19, we show the energy dependence of $\bar{p}/p, \bar{\Lambda}/\Lambda, \bar{H}e^3/He^3, \bar{H}e^4/He^4$ and $\bar{d}/d$ yield ratios over a very broad energy range. We take three times of volume and mass of each nucleon to calculate the volume and mass of He^3 in our calculation. Similarly, we calculate densities of other nuclei and hypernuclei using the similar method. We compare our results with the experimental data [74] and find a good agreement between these two. We stress that the agreement between the experimental and the calculated curves for the ratio $\bar{H}e^3/He^3$

is a powerful argument that indeed entropy conservation governs the production of light nuclei. In Fig. 20, we show the variations of $\Lambda/p, d/p$ with $\sqrt{s_{NN}}$. We compare our results with the experimental data points [74]. We also predict the energy dependence of nuclei as well as antinuclei yield ratio such as H_{Λ}^3/He^3 and $\bar{H}_{\bar{\Lambda}}^3/\bar{H}e^3$ over a broad energy range going from lower AGS energies to LHC energy. Some data have started appearing and we find that our model gives a good fit to the data.

V. CONCLUSIONS

In conclusion, we find that our model provides a good fit to the variations of total multiplicities as well as mid-rapidity densities of various particles and we deduce a large freeze-out volume of the fireball at RHIC energy and this picture supports the idea of a mixed phase after QGP formation before hadronization because a huge size of a homogeneous fireball source can only arise if a mixed phase has occurred before the formation of a hot, dense HG. Further, we present an analysis of rapidity distributions and transverse mass spectra of hadrons in central nucleus-nucleus collisions at various center-of-mass energies using our recently proposed equation of state (EOS). We see that the stationary thermal source alone cannot describe the experimental data fully unless we incorporate flow velocities in the longitudinal as well as in the transverse direction in our thermal model and as a result our modified model predictions show a good agreement with the experimental data. Our analysis shows that a collective flow develops at each $\sqrt{s_{NN}}$ which increases further with the increasing $\sqrt{s_{NN}}$. The description of the rapidity distributions and transverse mass spectra of hadrons at each $\sqrt{s_{NN}}$ matches very well with the experimental data. Although, we are not able to describe successfully the spectra for multistrange particles which suggests that a somewhat different type of mechanism is required. We find that the particle yields and ratios measured in heavy-ion collisions are described well by our thermal model and show an overwhelming evidence for chemical equilibrium at all beam energies. The rapidity distributions and transverse mass spectra which essentially are dependent on thermal parameters, also show a systematic behaviour and their interpretations most clearly involve the presence of a collective flow in the description of the thermal model. We have also found that our model together with a quasiparticle EOS for QGP gives the QCD phase boundary and the location of critical point almost overlapping on the freeze-out curve as predicted earlier

[34]. In conclusion, we find that our model provides an excellent description for the thermal and hadronic properties of the HG fireball and associated phase transitions existing in the ultra-relativistic heavy-ion collisions.

In summary, we have formulated a thermodynamically consistent EOS for a hot and dense HG fireball created in the ultra-relativistic heavy-ion collisions. We have incorporated a geometrical hard-core size for baryons and antibaryons only. In our description mesons may possess a size but they can penetrate and overlap on each other. Our prescription has also made use of full quantum statistics [5]. It is encouraging to note that our results for particle-ratios and their energy-dependence, total multiplicities, rapidity densities and rapidity and momentum spectra of various particles consistently match with the experimental data. We should emphasize that the hadrons emerging from a completely thermalized HG fireball do not give any information regarding a primordial QGP phase existing before HG. However, the large freeze-out volume of the fireball obtained in this analysis hints at a mixed phase occurring before pure HG phase.

VI. ACKNOWLEDGMENTS

S.K.T. and P.K.S. are grateful to the Council of Scientific and Industrial Research (CSIR), New Delhi, and University Grants Commission (UGC), New Delhi for providing research grants.

---

[1] C. P. Singh, Phys. Rept. 236, 147 (1993); Int. J. Mod. Phys. A 7, 7185 (1992).

[2] M. Gazdzicki, M. Gorenstein and P. Seyboth, Acta Physica Polonica B 42, 307 (2011).

[3] E. V. Shuryak, Phys. Rept. 61, 71 (1980).

[4] J. Letessier and J. Rafelski, Hadrons and Quark-Gluon Plasma, Cambridge University Press, U.K. (2004).

[5] S. K. Tiwari, P. K. Srivastava, and C. P. Singh, Phys. Rev. C 85, 014908 (2012).

[6] W. Busza and R. Leodoux, Ann. Rev. Nucl. Part. Sci. 36, 119 (1988).

[7] C. Blume and C. Markert, Prog. Part. Nucl. Phys. 66, 834 (2011).

[8] P. Huovinen, P. F. Kolb, and W. Heinz, Nucl. Phys. A 5, 698 (2002).

[9] L. D. Landau, Izv. Akad. Nauk. Sec. Fiz. 17, 51 (1953); J. D. Bjorken, Phys. Rev. D 27, 140 (1983).

[10] E. Schnedermann, J. Sollfrank, and U. Heinz, Phys. Rev. C 48, 2462 (1993).

[11] P. Braun-Munzinger *et al.*, Phys.Lett. B 365, 1 (1996); Phys. Lett. B 344, 43 (1995).

[12] E. Schnedermann, and U. Heinz, Phys. Rev. Lett. 69, 2908 (1992).

[13] S. Q. Feng, and Y. Zhong, Phys. Rev. C 83, 034908 (2011); S. Q. Feng and X. B. Yuan, Sci. China Ser. G 52, 198 (2009).

[14] T. Hirano, K. Morita, S. Muroya, and C. Nonaka, Phys. Rev. C 65, 061902 (2002); K. Morita, S. Muroya, C. Nonaka, and T. Hirano, ibid. 66, 054904 (2002).

[15] M. Gyulassy, P. Levai, and I. Vitev, Phys. Rev. Lett. 85, 5535 (2000); Nucl. Phys. B 594, 371 (2001).

[16] D. Kharzeev and M. Nardi, Phys. Lett. B 507, 121 (2001).

[17] J. Cleymans and K. Redlich, Phys. Rev. Lett. 81, 5284 (1998); J. Cleymans and H. Satz, Z. Phys.C 57, 135 (1993); J. Cleymans, H. Oeschler, and K. Redlich, Phys. Lett. B 485, 27 (2000); P. Braun-Munzinger, D. Magestro, K. Redlich, and J. Stachel, Phys. Lett. B 518, 41 (2001).

[18] D. H. Rischke, S. Bernard, and J. A. Maruhn, Nucl. Phys. A 595, 346 (1995); D. H. Rischke, Y. Pursun, and J. A. Maruhn, ibid.595, 383 (1995); 596, 717(E) (1996).

[19] S. A. Bass *et al.*, Prog. Part. Nucl. Phys. 41, 225 (1998).

[20] Y. M. Sinyukov, S. V. Akkelin, and Y. Hama, Phys. Rev. Lett. 89, 052301 (2002); S. V. Akkelin, M. S. Borysova, and Yu. M. Sinyukov, Acta Phys. Hung. A 22, 165 (2005).

[21] D. K. Srivastava, J. Alam, and B. Sinha, Phys. Lett. B 296, 11 (1992); D. K. Srivastava, J. Alam, S. Chakrabarty, B. Sinha, and S. Raha, Ann. Phys. 228, 104 (1993); D. K. Srivastava, J. Alam, S. Chakrabarty, S. Raha, and B. Sinha, Phys. Lett. B 278, 225 (1992).

[22] P. F. Kolb, U. W. Heinz, P. V. Ruuskanen, and S. A. Voloshin, Phys. Lett. B 503, 58 (2001); P. F. Kolb, P. Huovinen, U. W. Heinz, and H. Heiselberg, ibid. 500, 232 (2001); P. F. Kolb, U. W. Heinz, P. Huovinen, K. J. Eskola, and K. Tuominen, Nucl. Phys. A 696, 197 (2001).

[23] U. Mayer and U. Heinz, ibid. 56, 439 (1997); E. Schnedermann and U. Heinz, ibid. 50, 1675 (1994); U. Heinz, Nucl. Phys. A 661, 140c (1999).

[24] F. Becattini and J. Cleymans, J. Phys. G 34, S959 (2007); F. Becattini, J. Cleymans and J. Strumpfer, Proceeding of Science, (CPOD07), 012 (2007) [arXiv:0709.2599[hep-ph]].

[25] B. Biedron, and W. Broniowski, Phys. Rev. C 75, 054905 (2007); W. Broniowski and B. Biedron, J. Phys. G 35, 0440189 (2008).

[26] J. Cleymans, J. Strumpfer and L. Turko, Phys. Rev. C 78, 017901 (2008).

[27] W. Broniowski, and W. Florkowski, Phys. Rev. Lett. 87, 272302 (2001); Phys. Rev. C 65, 064905 (2002).

[28] D. Teaney, J. Lauret, and E. V. Shuryak, Phys. Rev. Lett. 86, 4783 (2001).

[29] C. Adler *et al.*, (STAR Collaboration), Phys. Rev. Lett. 87, 262302 (2001).

[30] K. Adcox *et al.*, (PHENIX Collaboration), Phys. Rev. Lett. 88, 242301 (2002).

[31] K. Adcox *et al.*, (PHENIX Collaboration), Phys. Rev. C 69, 024904 (2004).

[32] P. Bozek, Phys. Rev. C 77, 034911 (2008).

[33] C. P. Singh, B. K. Patra and K. K. Singh, Phys. Lett. B 387, 680 (1996).

[34] P. K. Srivastava, S. K. Tiwari, and C. P. Singh, Phys. Rev. D 82, 014023 (2010); Nucl. Phys. A 862-863 CF, 424 (2011) ; C. P. Singh, P. K. Srivastava and S. K. Tiwari, Phys. Rev. D 80, 114508 (2009); Phys. Rev. D 83, 039904 (E) (2011).

[35] P. K. Netrakanti, and B. Mohanty, Phys. Rev. C 71, 047901 (2005).

[36] P. V. Ruuskanen, Acta Physica Polonica B 18, 551 (1987).

[37] F. Cooper and G. Frye, Phys. Rev. D 10, 186 (1974).

[38] D. Adamova *et al.*, (CERES Collaboration), Phys. Rev. Lett. 90, 022301 (2003).

[39] F. Becattini *et al.*, Phys. Rev. C 64, 024901 (2001).

[40] J. L. Klay *et al.*, (E895 Collaboration), Phys. Rev. C 68, 054905 (2003).

[41] S. V. Afanasiev *et al.*, (NA49 Collaboration), Phys. Rev. C 66, 054902 (2002).

[42] M. Gazdzicki, (NA49 Collaboration), J. Phys. G, 30, S701 (2004).

[43] I. G. Bearden *et al.*, (BRAHMS Collaboration), Phys. Rev. Lett. 94, 162301 (2005).

[44] T. Anticic *et al.*, (NA49 Collaboration), Phys. Rev. Lett. 93, 022302 (2004).

[45] A. Richard *et al.*, (NA49 Collaboration), J. Phys. G, 31, S115 (2005).

[46] S. V. Afanasiev *et al.*, (NA49 Collaboration), Phys. Lett. B 491, 59 (2000).

[47] C. Meurer *et al.*, (NA49 Collaboration), J. Phys. G, 30, S1325 (2004).

[48] S. V. Afanasiev *et al.*, (NA49 Collaboration), Phys. Lett. B 538, 275 (2002).

[49] L. Ahle *et al.*, (E802 Collaboration), Phys. Rev. C 57, 466 (1998).

[50] L. Ahle *et al.*, (E866 and E917 Collaboration), Phys. Lett. B 476, 1 (2000).

[51] L. Ahle *et al.*, (E866 and E917 Collaboration), Phys. Lett. B 490, 53 (2000).

[52] L. Ahle *et al.*, (E802 Collaboration), Phys. Rev. C 58, 3523 (1998).

[53] C. Pinkenburg *et al.*, (E895 Collaboration), Nucl. Phys. A 698, 495c (2002).

[54] S. Albergo *et al.*, (E896 Collaboration), Phys. Rev. Lett. 88, 062301 (2002).

[55] P. Chung *et al.*, (E895 Collaboration), Phys. Rev. Lett. 91, 0202301 (2003).

[56] A. Andronic, P. Braun-Munzinger and J. Stachel, Nucl. Phys. A 772, 167 (2006).

[57] M. M. Aggarwal *et al.*, (STAR Collaboration), Phys. Rev. C 83, 024901 (2011).

[58] M. Mishra and C. P. Singh, Phys. Rev. C 76, 024908 (2007); Phys. Rev. C 78, 024910 (2008); Phys. Lett. B 651, 119 (2007).

[59] I. G. Bearden *et al.*, (BRAHMS Collaboration), Phys. Rev. Lett. 94, 162301 (2005).

[60] S. V. Afanasiev *et al.*, (NA49 Collaboration), Phys. Rev. C 66, 054902 (2002).

[61] I. G. Bearden *et al.*, (BRAHMS Collaboration), Phys. Rev. Lett. 93, 102301 (2004).

[62] H. Yang, J. Phys. G, 35, 104129 (2008).

[63] S. S. Adler *et al.*, (PHENIX Collaboration), Phys. Rev. C 69, 034909 (2004).

[64] B. I. Abelev *et al.*, (STAR Collaboration), Phys. Rev. C 79, 064903 (2009).

[65] M. Floris, (ALICE collaboration), arXiv:1108.3257v1[hep-ex].

[66] C. Shen, U. Heinz, P. Huovinen, and H. Song, Phys. Rev. C 84, 044903 (2011).

[67] A. Andronic, P. Braun-Munzinger and J. Stachel, Nucl. Phys. A 772, 167 (2006).

[68] M. Bleicher *et al.*, J. Phys. G 25, 1859 (1999).

[69] P. J. Siemens, and J. I. Kapusta, Phys. Rev. Lett. 43, 1486 (1979).

[70] D. Hahn, and H. Stöcker, Nucl. Phys. A 476, 718 (1988).

[71] P. Braun-Munzinger, and J. Stachel, J. Phys. G 21, L17 (1995).

[72] P. Braun-Munzinger, and J. Stachel, J. Phys. G 28, 1971 (2002).

[73] B. I. Abelev *et al.*, (STAR Collaboration), Science 328, 58 (2010).

[74] A. Andronic, P. Braun-Munzinger, J. Stachel, and H. Stöcker, Phys. Lett. B 697, 203 (2011).